Non-Newtonian rheology in a capillary tube with varying radius

Federico Lanza, Alberto Rosso, Laurent Talon, Alex Hansen

Non-Newtonian rheology in a capillary tube with varying radius

Federico Lanza[1,2*], Alberto Rosso[1], Laurent Talon[3] and Alex Hansen[2]

[1]LPTMS, CNRS, Université Paris-Saclay, 91405, Orsay, France.
[2]PoreLab, Department of Physics, Norwegian University of Science and Technology, N-7491, Trondheim, Norway.
[3]FAST, CNRS, Université Paris-Saclay, 91405, Orsay, France.

*Corresponding author(s). E-mail(s): federico.lanza@universite-paris-saclay.fr;
Contributing authors: alberto.rosso@universite-paris-saclay.fr; laurent.talon@universite-paris-saclay.fr; alex.hansen@ntnu.no;

Abstract

Fluid blobs in an immiscible Newtonian fluid flowing in a capillary tube with varying radius show highly non-linear behaviour. We consider here a generalization of previously obtained results to blobs of non-Newtonian fluids. We compute here the yield pressure drop and the mean flow rate in two cases: (i) when a single blob is injected, (ii) when many blobs are randomly injected into the tube. We find that the capillary effects emerge from the non-uniformity of the tube radius and contribute to the threshold pressure for flow to occur. Furthermore, in presence of many blobs the threshold value depends on the number of blobs and their relative distances which are randomly distributed. For a capillary fiber bundle of identical parallel tubes, we calculate the probability distribution of the threshold pressure and the mean flow rate. We consider two geometries: tubes of sinusoidal shape, for which we derive explicit expressions, and triangular-shaped tubes, for which we find that essential singularities are developed. We perform numerical simulations confirming our analytical results.

Keywords: Non-Newtonian fluids, Immiscible two-phase flow, Capillary tube, Capillary fiber bundle model

Introduction

In many industrial, geophysical or biological applications related to porous media, non-Newtonian fluids are frequently encountered. Indeed many complex fluids present a non-linear rheology as for example slurries, heavy oils, suspensions (Barnes et al, 1989; Coussot, 2005) or some biological fluids like blood (Popel and Johnson, 2005; Bessonov et al, 2016). Here, we are interested in yield stress fluids, which require a minimal applied stress to flow. These fluids are involved in many practical applications, such as drilling for oil extraction, where proppant fluids are injected in the soil for the fracking process (Barbati et al, 2016), stabilization of bone fractures in biomedical engineering (Widmer Soyka et al, 2013), or ground reinforcement by cement injection. Yield stress fluids in porous media is a challenging and interesting problem which has been the subject of many studies in the last decades (Entov, 1967; Park et al, 1973; Al-Fariss and Pinder, 1987; Chen et al, 2005; Sochi and Blunt, 2008; Talon and Bauer, 2013; Rodríguez de Castro and Radilla, 2017; Liu et al, 2019). Because of the presence of a yield stress, the fluid is able to flow only if a certain amount of pressure is imposed (Roux and Herrmann, 1987; Chen et al, 2005; Liu et al, 2019; Fraggedakis et al, 2021). There is then a strong coupling between the rheology of the fluid and the disorder of the porous structure, implying that some regions are easier to yield than others. Above this pressure threshold, as demonstrated by several studies (Roux and Herrmann, 1987; Talon and Bauer, 2013; Chevalier and Talon, 2015; Waisbord et al, 2019; Liu et al, 2019), a progressive increase of flowing paths occurs. As a consequence, the flow rate Q increases with the applied pressure drop ΔP according to a power-law:

$$Q \propto (\Delta P - \Delta P_c)^{\beta}, \tag{1}$$

where ΔP_c is a pressure drop threshold and β a characteristic exponent to be determined. The origin of this flowing regime is an effect of the disorder, but remarkably the value of the exponent $\beta = 2$ found in a recent work by Liu et al (2019) for 2D porous media is independent from the type of disorder.
This is however not the case in 1D, if one describes the porous media by a series of uniform bundle of capillaries. The flow curve above the threshold depends then on the details of the opening distribution (Nash and Rees, 2016).
If the flow of yield stress fluids in porous media is already a challenging problem, in many situations the complexity is increased by the presence of different immiscible fluids. Multi-phase flow in porous media is a very old and rich subject, and is still the topic of many ongoing research. One of the main difficulties lies in the presence of numerous interfaces exerting capillary forces on the fluids present, which makes the dynamic very non-linear. It is then surprising that, during many decades, the models predicting the mean flow rate as function of the mean applied pressure has assumed linear relations (Bear, 1988; Dullien, 1991).
In the last decade, however, a series of experiments and simulations (Tallakstad et al, 2009; Rassi et al, 2011; Sinha and Hansen, 2012; Yiotis et al, 2013;

Chevalier et al, 2015; Zhang et al, 2021) have shown the existence of a non-linear flowing regime at low flow rate. Similarly to the yield stress fluid case, the physical reason behind this observation lies in the presence of the heterogeneity. In fact, due to capillary forces the interfaces can only move if a certain pressure is applied. In a disordered media, certain regions allows the movement of interfaces more easily than others. At very low applied pressure, the displacement of the interfaces occurs only in few pathways whose number rises with the applied pressure (Yiotis et al, 2019). This increase is then responsible for a non-linear flow rate-pressure relationship similar to eq. (1), where the exponent β has been reported to vary in the range $\beta \in [1.5, 2]$ depending on the flow condition (Tallakstad et al, 2009; Yiotis et al, 2013; Rassi et al, 2011; Sinha and Hansen, 2012; Sinha et al, 2017; Yiotis et al, 2019; Zhang et al, 2021). An argument based on comparing length scales associated with the viscous forces with those set by the capillary forces gave $\beta = 2$ (Tallakstad et al, 2009). This value was also found using a mean field theory-based calculation (Sinha and Hansen, 2012), whereas a calculation based on the capillary fiber bundle model, gives either $\beta = 3/2$ or $\beta = 2$ depending on the statistical distribution of the flow thresholds (Roy et al, 2019). These approaches are all based on the mobilization of interfaces and can be understood for instance by considering many blobs in a single 1D pore with spatial varying opening. In this case, there exists a minimal pressure threshold to initiate the flow. Above, the flow rate increases with a power-law as eq. (1), similarly to a Herschel-Bulkley yield stress fluid with index $n = 1/\beta$. Aursjø et al (2014) found the values $\beta = 1.49$ and 1.35 for a two-dimensional porous model where transport of one of the fluids occurs entirely through film flow, depending on the fractional flow rate.

In this work, we aim to investigate two-phase flows, but in the case where one of the two fluids presents a yield threshold. The situation is then more complex as both the rheology and the surface tension lead to a threshold pressure to initiate the flow. For simplification, we propose to model a porous medium by a set of identical capillaries with varying opening (i.e., the capillary fiber bundle model, see Scheidegger (1953, 1974)). The first question we want to address is the determination of the pressure threshold depending on the rheology, the surface tension and the disorder of the capillaries. The second question is then to determine the flow curve just above this threshold. We will show that the flow rate follows a power law, and we will determine the exponent depending the structure disorder.

For a Newtonian fluid in a cylindrical capillary tube, neglecting inertia, the volumetric flow rate, q, is expected to grow linearly with the pressure gradient $\Delta P/l$. Here $\Delta P = P_{\text{in}} - P_{\text{out}}$ is the pressure difference applied to the edges of a tube of length l (in the following we assume $\Delta P > 0$ for simplicity). This behaviour is given by the celebrated Poiseuille law $q = \pi r_0^4 \Delta P/(8\mu l)$, where μ is the fluid viscosity and r_0 the tube radius. However, non-Newtonian yield stress fluids display a non-linear response. Their rheology can be modeled by

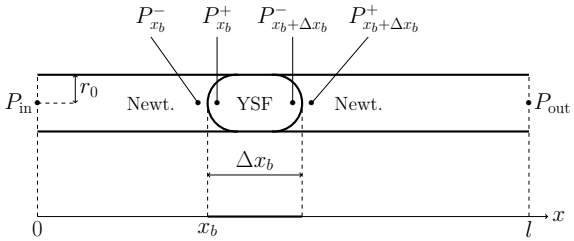

Fig. 1 Two-dimensional sketch of a blob of yield stress fluid in a uniform tube. On the x-axis, the one-dimensional model relative to the problem is pictured, where the thick line is the projection along x of the yield stress blob, while the thin line represent the part occupied by the Newtonian fluid.

the Herschel–Bulkley constitutive equation (Bird, 1976), that gives a relation between the shear stress τ applied to the fluid and the shear rate $\dot{\gamma}$

$$\tau = \tau_y + k\dot{\gamma}^n, \tag{2}$$

The constant k is the consistency, the exponent $n > 0$ is the flow index and τ_y is the yield stress. In this case the flow in the tube occurs only above an yield pressure drop ΔP_c, and the flow rate grows with pressure in a non-linear way. For example, for a perfect cylindrical tube filled with a non-Newtonian yield stress fluid, the yield pressure is $\Delta P_c = 2\tau_y l/r_0$ and the flow law (Bird et al, 1987):

$$q = \begin{cases} C_0\, r_0^{4+\frac{1}{n}} \left(\frac{\Delta P - \Delta P_c}{l}\right)^{\frac{1}{n}+1} & \text{if } \Delta P \to \Delta P_c^+, \\ \\ C_\infty\, r_0^{3+\frac{1}{n}} \left(\frac{\Delta P - \Delta \widetilde{P}_c}{l}\right)^{\frac{1}{n}} & \text{if } \Delta P \gg \Delta P_c, \end{cases} \tag{3}$$

here $C_0 = n\pi/((n+1)2^{1+1/n}k^{1/n}\tau_y)$, $C_\infty = n\pi/((3n+1)(2k)^{1/n})$ and $\Delta\widetilde{P}_c = ((3n+1)/(2n+1))\Delta P_c$ is a pseudo critical pressure (see Talon et al (2014); Bauer et al (2019)).

1 Model for a single blob

1.1 Uniform tube

We now consider the case of a cylindrical tube with constant radius filled with a Newtonian liquid, in which one small blob of yield stress fluid (YSF) is injected, as pictured in Figure 1. We assume the fluids to be immiscible and incompressible. The blob, of size $\Delta x_b \ll l$ and position x_b, is at the origin of a critical yield pressure $\Delta P_c = P_y^0 = 2\tau_y \Delta x_b/r_0$. The total pressure drop ΔP needed to sustain a flow rate q can be expressed as the sum of the pressure drops across every portion of fluid. We call $P^-_{x_b}$ and $P^+_{x_b}$, respectively, the pressure value just before and just after the left surface separating the Newtonian fluid from the blob (positioned at x_b), while $P^-_{x_b+\Delta x_b}$ and $P^+_{x_b+\Delta x_b}$

will be, respectively, the pressure just before and just after the right surface (positioned at $x_b+\Delta x_b$). The pressure drops across both portions of Newtonian fluid, in the intervals $0 < x < x_b$ and $x_b + \Delta x_b < x < l$, are given by the Poiseuille law

$$\begin{aligned} P_{\text{in}} - P^-_{x_b} &= q\frac{8\mu x_b}{\pi r_0^4}, \\ P^+_{x_b+\Delta x_b} - P_{\text{out}} &= q\,\frac{8\mu(l - x_b - \Delta x_b)}{\pi r_0^4}. \end{aligned} \tag{4}$$

The pressure drop across the blob is instead given by Equation (3) and writes

$$P^+_{x_b} - P^-_{x_b+\Delta x_b} = \begin{cases} \left(\frac{q}{C_0\, r_0^{4+\frac{1}{n}}}\right)^{\frac{n}{n+1}} \Delta x_b + \Delta P_c \quad \text{if } \Delta P \to \Delta P_c^+, \\ \\ q^n \frac{\Delta x_b}{C_\infty^n r_0^{3n+1}} + \Delta \widetilde{P}_c \qquad \text{if } \Delta P \gg \Delta P_c \end{cases} \tag{5}$$

Moreover, when two immiscible fluids are in contact, at the interface emerges a discontinuity in pressure, called capillary pressure, whose sign depends on the curvature of the interface (Bear, 1988). Hence, in a perfect cylindrical tube, the total capillary pressure across the two interfaces of a blob cancels out since at each interface the capillary pressure discontinuity is $2\sigma/r_0$ (σ being the surface tension between the two fluids)[1], but the signs of the two contributions are opposite as the two interfaces have opposite curvature.
The sum of the three pressure drops given in equations (4) and (5) in the limit $\Delta P \gtrsim \Delta P_c$ is then

$$\Delta P = q\frac{8\mu(l - \Delta x_b)}{\pi r_0^4} + q^{\frac{n}{n+1}} \frac{\Delta x_b}{C_0^{\frac{n}{n+1}} r_0^{\frac{4n+1}{n+1}}} + \Delta P_c. \tag{6}$$

In this limit the flow vanishes to 0, so we can neglect the linear term in equation (6) as $n/(n+1) < 1 \;\forall\; n > 0$.
In the opposite limit $\Delta P \gg \Delta P_c$ we have

$$\Delta P = q\frac{8\mu(l - \Delta x_b)}{\pi r_0^4} + q^n \frac{\Delta x_b}{C_\infty^n r_0^{3n+1}} + \Delta \widetilde{P}_c. \tag{7}$$

Since now $q \to \infty$, we should distinguish between a shear-thinning fluid and a shear-thickening fluid, for which $n < 1$ and $n > 1$ respectively. In the first case, the leading term is the one proportional to q^n, while in the other case the leading term is the linear one. Finally, we can write the volumetric flow

[1] Here we implicitly assume the contact angle between the meniscus and the tube to be small such that the radius of the spherical interface is approximately equal to the radius of the tube.

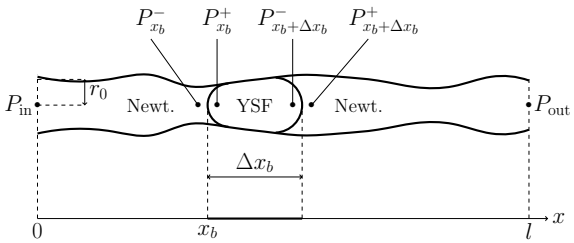

Fig. 2 Two-dimensional sketch of a blob of yield stress fluid in a non-uniform tube. On the x-axis, the one-dimensional model relative to the problem is pictured, where the thick line is the projection along x of the yield stress blob, while the thin line represent the part occupied by the Newtonian fluid.

rate in the two different limits:

$$q(\Delta P) = \begin{cases} C_0\, r_0^{4+\frac{1}{n}} \left(\frac{\Delta P - \Delta P_c}{\Delta x_b}\right)^{1+\frac{1}{n}} & \text{if } q \to 0 \\ \begin{cases} C_\infty r_0^{3+\frac{1}{n}} \left(\frac{\Delta P - \Delta \widetilde{P}_c}{\Delta x_b}\right)^{\frac{1}{n}} & \text{if } n < 1 \\ \frac{\pi r_0^4}{8\mu} \frac{\Delta P - \Delta \widetilde{P}_c}{l - \Delta x_b} & \text{if } n > 1 \end{cases} & \text{if } q \to +\infty \end{cases} \tag{8}$$

1.2 Non-uniform tube

We consider now a tube still of length l, but with varying radius $r(x)$ (see figure 2) described by the following equation

$$r(x) = \frac{r_0}{1 + a f(x/r_0)}, \tag{9}$$

where $f(x/r_0)$ is a bounded function with zero average in the interval $x/r_0 \in [0, l/r_0]$, $a \ll 1$ a dimensionless constant and r_0 a characteristic radius.
In this work, we will assume that the radius varies slowly enough that the radial component of the fluid velocity can be neglected compared to the axial component $f' \ll 1$. The size of the blob Δx_b can also be considered constant along the tube. This hypothesis, also named lubrication approximation, is usually used in heterogeneous tube or fracture (Brown, 1987) as it allows to determine the flow rate as function of the local gradient of pressure (Happel and Brenner, 1983).
For Newtonian fluids, this approximation holds for a sufficiently slow variation of the radius (Happel and Brenner, 1983; Malevich et al, 2006). For yield stress fluid, a mathematical criterion of application remains an open question. This approximation has however been successfully applied in many pore network models for Newtonian and non-Newtonian fluids (for example: Lopez et al (2003); Balhoff and Thompson (2004); Sochi and Blunt (2008)).

Indeed, this approximation allows to determine a general relationship between pressure drop and flow rate. Even when the condition of applicability is not fullfilled, the deviation to the lubrication prediction can then be circumvented by introducing an effective hydraulic radius (Dullien (1991)). For yield stress fluids, the lubrication approximation is more complicated (see Frigaard and Ryan (2004)). For example, Roustaei et al (2016) study the flow-pressure relationship for Bingham fluid in different heterogeneous fractures. The flow-pressure relationship is affected by two other mechanisms. First, the lubrication approximation predicts an unyielded plug in the center that breaks when the variation in opening is too large. More important is the presence of a unyielded "fouling" layer at the wall. Interestingly, this layer tends to smooth out the effect of the heterogeneity of the opening. As in the Newtonian case, it follows that even if the lubrication approximation does not hold, the flow-pressure relationship can be approximated by an equation like eq. (3) providing the introduction of an equivalent radius distribution.

1.2.1 Analytic radius variability

Let's assume $f(x/r_0)$ to be analytic in $x \in [0, l]$. Two modifications should be included with respect to the uniform case. First, the capillary pressure across the blob interfaces do not cancel anymore (Sinha et al, 2013). Since $P^-_{x_b} - P^+_{x_b} = 2\sigma/r(x_b)$ and $P^+_{x_b+\Delta x_b} - P^-_{x_b+\Delta x_b} = 2\sigma/r(x_b+\Delta x_b)$, their difference is in general non zero and approximately equal to

$$\frac{2\sigma}{r(x_b)} - \frac{2\sigma}{r(x_b+\Delta x_b)} \simeq a\frac{P_\sigma \Delta x_b}{r_0} f'(x_b/r_0), \tag{10}$$

with $P_\sigma = 2\sigma/r_0$ and $f'(x_b/r_0)$ the derivative of f at x_b. Secondly, as $r(x)$ is non-constant, both Poiseuille law and Eq. (3) can be considered valid only along infinitesimal intervals of length dx. For both reasons, the flow rate varies in time as a function of the blob location x_b. The Poiseuille equation becomes $q(x_b) = -\pi r(x)^4 (dP/dx)/(8\mu)$ from which, integrating along both portions of Newtonian fluids, at the first order of a we get:

$$P_{\text{in}} - P^-_{x_b} = q(x_b)\,\frac{8\mu}{\pi r_0^4}\left(x_b + 4a\int_0^{x_b} f(x/r_0)dx\right), \tag{11}$$

$$P^+_{x_b+\Delta x_b} - P_{\text{out}} = q(x_b)\,\frac{8\mu}{\pi r_0^4}\left(l - x_b - \Delta x_b + 4a\int_{x_b+\Delta x_b}^{l} f(x/r_0)dx\right) \tag{12}$$

Considering the limit $\Delta P \to \Delta P_c^+$, eq. (3) becomes instead $q(x_b) = C_0\, r(x)^{4+\frac{1}{n}} \left(dP/dx - 2\tau_y/r(x)\right)^{\frac{1}{n}+1}$, which, integrated along the blob interval, gives:

$$P^+_{x_b} - P^-_{x_b+\Delta x_b} \simeq \left(\frac{q(x_b)}{C_0\, r_0^{4+\frac{1}{n}}}\right)^{\frac{n}{n+1}} \Delta x_b + P_y^0\left[1 + a f(x_b/r_0)\right],$$

where $P_y^0 = 2\tau_y \Delta x_b / r_0$. Note that we approximated the integral:

$$\int_{x_b}^{x_b+\Delta x_b} \frac{1}{r^{4+1/n}(x)} dx \simeq \frac{1}{r_0^{4+1/n}} \Delta x_b, \tag{13}$$

because the correction only affects the prefactor of the flow curve, and not the exponent or the threshold. Since in this limit $q(x_b) \ll 1$, the leading behavior of the flow curve can be written as:

$$q(x_b) \simeq C_0 \, r_0^{4+\frac{1}{n}} \left[\frac{\Delta P - \gamma(x_b/r_0)}{\Delta x_b} \right]^{1+\frac{1}{n}}, \tag{14}$$

where we have defined the function:

$$\gamma(x_b/r_0) = P_y^0 + a \left[P_y^0 f(x_b/r_0) + P_\sigma \frac{\Delta x_b}{r_0} f'(x_b/r_0) \right]. \tag{15}$$

From eq. (14) we note that in a deformed tube the critical pressure drop ΔP_y above which flow is possible has increased with respect to the cylindrical tube, and is equal to the maximum of $\gamma(x_b)$:

$$\Delta P_c = P_y^0 + a \max_{0<x_b<l} \left[P_y^0 f(x_b/r_0) + P_\sigma \frac{\Delta x_b}{r_0} {}_0 f'(x_b/r_0) \right], \tag{16}$$

$$= P_y^0 \left\{ 1 + a \max_{0<x_b<l} \left[f(x_b/r_0) + \frac{\sigma}{r_0 \tau_y} f'(x_b/r_0) \right] \right\}; \tag{17}$$

we denote x_m the position of such maximum along the tube. Three terms contribute to the critical pressure. The first constant one is due to the yield threshold. The second is also due to the yield stress, but depends on the tube shape. The last one, related to the capillary force, is based on the derivative of f. The competition between the last two terms is then governed by the ratio between the relative derivative f/f' and the dimensionless number $\frac{P_\sigma \Delta x_b}{P_y^0 r_0} = \frac{\sigma}{r_0 \tau_y}$.

The blob position moves as $dx_b/dt = q/(\pi r_0^2)$, hence from eq. (14) we get the equation of motion

$$\frac{dx_b}{dt} = \frac{C_0 \, r_0^{2+\frac{1}{n}}}{\pi \Delta x_b^{1+\frac{1}{n}}} \left[\Delta P - \gamma(x_b/r_0) \right]^{1+\frac{1}{n}}. \tag{18}$$

The time T needed for the blob to move from one end of the tube to the other can be computed from (18):

$$T = \int_0^l \frac{dx_b}{dx_b/dt} \propto \int_0^l \frac{dx_b}{[\Delta P - \gamma(x_b/r_0)]^{1+\frac{1}{n}}}. \tag{19}$$

In general $\gamma(x_b/r_0)$ relies on the specific form of $f(x_b/r_0)$. However, supposing that $f(x_b/r_0)$ is analytical, we can expand $\gamma(x_b/r_0)$ around x_m: $\gamma(x_b/r_0) = \Delta P_c - \alpha(x_b - x_m)^2 + \dots$
For $\Delta P \to \Delta P_c^+$, the dominant contribution to the integral of eq. (19) is around x_m, so we can write

$$T \propto \int_0^l \frac{dx_b}{[\Delta P - \Delta P_c + \alpha(x_b - x_m)^2]^{1+\frac{1}{n}}} \propto (\Delta P - \Delta P_c)^{-\left(\frac{1}{n}+\frac{1}{2}\right)}. \tag{20}$$

The flux averaged over the time T, $\langle q \rangle_T$ is then

$$\langle q \rangle_T = \frac{\pi r_0^2 l}{T} \propto (\Delta P - \Delta P_c)^{\frac{1}{n}+\frac{1}{2}}. \tag{21}$$

Note that close to the yield threshold ΔP_c, the power-law exponent $1/n + 1/2$ of the flow rate turns out to be different from $1 + 1/n$ in eq. (8) for the uniform tube.
On the other hand, in the opposite limit $\Delta P \gg \Delta P_c$, since the fluctuations along the critical pressure are negligible, we expect the same behaviour of the cylindrical tube.

1.2.2 Non-analytic radius variability

As a final remark, we discuss the case where $f(x_b/r_0)$ is not analytic. In the framework of the fiber bundle model, capillary tubes presenting non analytic points allows to model porous materials presenting a rough and angular microstructure, e.g. matrices of randomly packed grains of quartz sand (Xiong et al, 2019). The non-linear prediction of eq. (21) hold only if $\gamma(x_b/r_0)$ is derivable at least twice. Otherwise, its expansion around x_m is of the form: $\gamma(x_b) = \Delta P_c + \alpha|x_b - x_m|^\delta + \dots$, with $\delta > 0$. In this case, the behavior of the integral in eq. (20) is modified and the flux averaged over T is then

$$\langle q \rangle_T \propto (\Delta P - \Delta P_c)^{\frac{1}{n}+1-\frac{1}{\delta}}. \tag{22}$$

To provide a concrete example, we consider a saw-tooth triangular geometry:

$$f\left(\frac{x}{r_0}\right) = \frac{4r_0}{l}\left|\frac{x}{r_0} - \frac{l}{2r_0}\right| - 1, \quad x \in]0, l]\,. \tag{23}$$

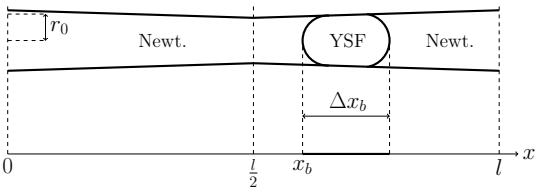

Fig. 3 Two-dimensional sketch of a blob of yield stress fluid in a triangular tube. On the x-axis, the one-dimensional model relative to the problem is pictured, where the thick line is the projection along x of the yield stress blob, while the thin line represent the part occupied by the Newtonian fluid.

A sketch of such geometry is shown in Figure 3. In this case we have

$$\begin{aligned}\gamma(x_b/r_0) &= P_y^0 + \frac{4ar_0}{l}\left[P_y^0\left|\frac{x_b}{r_0} - \frac{l}{2r_0}\right| + P_\sigma\frac{\Delta x_b}{r_0}\,\mathrm{sgn}\left(\frac{x_b}{r_0} - \frac{l}{2r_0}\right)\right] \\ &= P_y^0\left\{1 + \frac{4ar_0}{l}\left[\left|\frac{x_b}{r_0} - \frac{l}{2r_0}\right| + \frac{\sigma}{\tau_y r_0}\,\mathrm{sgn}\left(\frac{x_b}{r_0} - \frac{l}{2r_0}\right)\right]\right\}\end{aligned}$$

Its maximum is located at the discontinuity point $x_m = l$ and writes

$$\begin{aligned}\Delta P_c &= P_y^0 + a\left[2P_y^0 + \frac{4}{l}P_\sigma\Delta x_b\right] \\ &= P_y^0\left\{1 + 2a\left[1 + \frac{2\sigma}{\tau_y l}\right]\right\}.\end{aligned} \tag{24}$$

Integrating eq. (19) yields to $\delta = 1$ if the blob fluid presents yield stress, while $\langle q\rangle_T \propto (\Delta P - \Delta P_c)^{\frac{1}{n}+1}$ in absence of yield stress ($P_y^0 = 0$).

2 Model for many blobs

In a uniform tube, the flow curve obtained when a single shot of non-Newtonian fluid is injected is identical to the one obtained when the same amount of fluid is split in N small blobs. This is not the case for a non-uniform tube. To be concrete, we address the case of several identical blobs of non-Newtonian fluid (see figure 4). It comes out that the critical pressure obtained with N blobs of length Δx_b is larger than $NP_y^0 = 2N\Delta x_b\,\tau_y/r_0$, the value expected for a single shot of length equal to $N\Delta x_b$. The difference depends on the total number of blobs and on the specific blob configuration.

During the flow, the relative distances between different blobs remain constant as the fluids are incompressible. Moreover, periodic boundary conditions are set, namely $f(x/r_0) = f\left(\frac{x+l}{r_0}\right)$. This assumption can describe two different situations: (i) a tube of length l with periodic boundary conditions (ii) a tube of length $L \gg l$ presenting a periodic deformation of spatial period l. In the latter case, the blobs are in general located on different periods, but it is convenient to shift their position in the first period: more precisely, if a blob is located

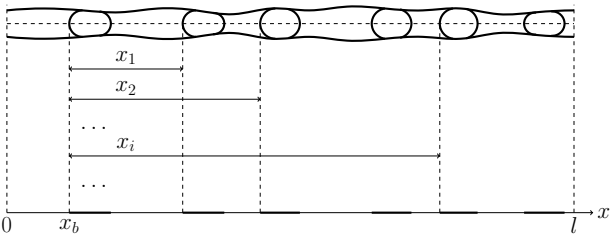

Fig. 4 Two-dimensional sketch of several blobs of yield stress fluid in a non-uniform tube of length l. On the x-axis, the one-dimensional model relative to the problem is pictured, where the thick line is the projection along x of the yield stress blobs, while the thin line represent the part occupied by the Newtonian fluid.

at a certain position in the k-th period, the dynamics of the system does not change if we subtract the quantity $(k-1)l$ from that position. We then denote with x_b the position of the most left blob and with x_i the distance from its i-th blob neighbour. Thus $i = 1, \dots, N-1$, and the i-th right neighbour is located at $x_b + x_i$. When x_b moves from 0 to l all the other blobs move exactly one period.
In the limit of small flow rate $q \to 0$, the pressure drop at the edges of the i-th blob is

$$P^+_{x_b+x_i} - P^-_{x_b+x_i+\Delta x_b} = \Delta x_b \left(\frac{q}{C_0 r_0^{4+\frac{1}{n}}} \right)^{\frac{n}{n+1}} + P_y^0 + a P_y^0 f\left(\frac{x_b + x_i}{r_0} \right). \quad (25)$$

At this, one must add the capillary pressure drop $aP_\sigma \frac{\Delta x_b}{r_0} f'(\frac{x_b+x_i}{r_0})$. Summing the contributions of all the N blobs and neglecting the pressure drop induced by the Newtonian fluid, we obtain the following flow rate equation, that depends not only on the variable x_b, but also on the set of constant values $\{x_i\}$:

$$q(x_b; \{x_i\}) = C_0 r_0^{4+\frac{1}{n}} \left[\frac{\Delta P - \gamma(x_b/r_0; \{x_i/r_0\})}{N \Delta x_b} \right]^{\frac{1}{n}+1}, \quad (26)$$

with

$$\gamma\left(\frac{x_b}{r_0}; \left\{ \frac{x_i}{r_0} \right\} \right) = N P_y^0 + a \left[P_y^0 F\left(\frac{x_b}{r_0}; \left\{ \frac{x_i}{r_0} \right\} \right) + P_\sigma \frac{\Delta x_b}{r_0} F'\left(\frac{x_b}{r_0}; \left\{ \frac{x_i}{r_0} \right\} \right) \right], \quad (27)$$

where the function

$$F\left(\frac{x_b}{r_0}; \left\{ \frac{x_i}{r_0} \right\} \right) = f(x_b/r_0) + \sum_{i=1}^{N-1} f\left(\frac{x_b + x_i}{r_0} \right), \quad (28)$$

and $F'(y; \{\frac{x_i}{r_0}\})$ is the first derivative of $F(y; \{\frac{x_i}{r_0}\})$ with respect to y. The critical pressure ΔP_c needed for the system to flow is then given by the maximum

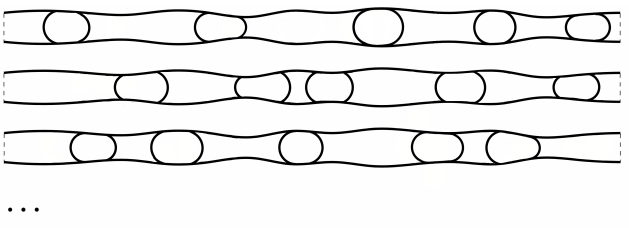

Fig. 5 Sketch of a fiber bundle of identically shaped tubes, each filled with blobs randomly located along it.

of $\gamma(\frac{x_b}{r_0}, \{\frac{x_i}{r_0}\})$ in the interval $0 < x_b < l$:

$$\Delta P_c\left(\left\{\frac{x_i}{r_0}\right\}\right) = \max_{0\le x_b<l}\left[\gamma\left(\frac{x_b}{r_0}, \left\{\frac{x_i}{r_0}\right\}\right)\right]. \tag{29}$$

From eq. (29) we can see that the value of the critical pressure relies thus not only on the number of blobs, but also on the specific configuration of the blobs position along the tube, namely on their distances $\{x_i\}$.

Since there is no preferred position of the blobs along the tube, the most important configuration is the one where the positions of the blobs are uniformly (evenly) distributed. In the diluted limit where $N\Delta x_b$ is very small compared to the tube length, the position of every blob shifted in the first period is uniformly distributed in the interval $(0, l)$. Our first goal is to compute the probability distribution function of the critical pressure, $\Pi(\Delta P_c)$, associated to such ensemble.

The second goal is to characterize the flow rate. Again the flow of a given tube averaged over a period, $\langle q\rangle_T = \langle q(\{x_i\})\rangle_T$, depends on its specific blobs configuration, and thus on its pressure threshold value $\Delta P_c = \Delta P_c(\{x_i\})$. For $\Delta P \to \Delta P_c^+$:

$$T \propto \int_0^l \frac{dx_b}{\left[\Delta P - \gamma\left(\frac{x_b}{r_0}; \left\{\frac{x_i}{r_0}\right\}\right)\right]^{1+\frac{1}{n}}} \propto (\Delta P - \Delta P_c)^{-\left(\frac{1}{n}+\frac{1}{2}\right)} \tag{30}$$

and thus $\langle q\rangle_T \propto (\Delta P - \Delta P_c)^{1/n+1/2}$ if the tube modulation is analytical, or, more generally, $\langle q\rangle_T \propto (\Delta P - \Delta P_c)^{1/n+1-1/\delta}$.

Once these two quantities are obtained, we can calculate the flow rate in a fiber bundle model (Roy et al, 2019), in which the same pressure drop ΔP is applied to many tubes which are identically shaped. Each tube is assumed to be filled with a Newtonian liquid together with N blobs injected at random positions along the tube, as pictured in Figure 5. In the limit of many tubes, the mean flow rate averaged over a period is obtained by averaging over all possible configurations of the blobs positions. We will call it $\overline{\langle q\rangle_T}$, where the overline denotes the average over the blob configurations. For ΔP slightly greater than

NP_y^0, we expect that the flow rate of every tube of the fiber bundle follows the small flow power-law exponent $1/n + 1 - 1/\delta$ if the pressure drop applied is greater than the pressure threshold of that tube, namely $\Delta P > \Delta P_c$, or is null if on the contrary $\Delta P \leq \Delta P_c$. Instead, we have tubes in the large flow limit, whose flow rate is described by the second case of eq. (8), only if ΔP is sufficiently greater than $\widetilde{\Delta} P_c = ((3n+1)/(2n+1))NP_y^0$. Since $NP_y^0 < \Delta\widetilde{P}_c < (3/2)NP_y^0$ for all $n > 0$, there's always a finite range of values of ΔP for which all tubes in the bundle presenting non-null flow obey to the small flow regime. Moreover, $\Delta P_c \geq NP_y^0$ but is typically much lower than $\Delta\widetilde{P}_c$, because the fluctuations on the value of ΔP_c are smaller than the difference between NP_y^0 and $\Delta\widetilde{P}_c$. The effects on the mean flow rate caused by the non-uniformity of the tubes can then be seen only if ΔP is sufficiently close to NP_y^0. In this limit we can compute the mean flow rate per tube as

$$\overline{\langle q \rangle_T} \propto \int_{NP_y^0}^{\Delta P} d\Delta P_c \, \Pi(\Delta P_c)(\Delta P - \Delta P_c)^{\frac{1}{n}+1-\frac{1}{\delta}}. \tag{31}$$

2.1 Sinusoidal geometry

In this section, we study the case

$$f(x/r_0) = \cos\left(2\pi x/l\right). \tag{32}$$

It is useful to introduce the angle variables $\theta_b = 2\pi\frac{x_b}{l}$ and $\theta_i = 2\pi\frac{x_i}{l}$. Using the trigonometric relations, we can write

$$F(\theta_b; \{\theta_i\}) = \cos(\theta_b) + \sum_{i=1}^{N-1} \cos(\theta_b + \theta_i) = \sqrt{N} A \cos(\theta_b + \phi) \tag{33}$$

where the amplitude is

$$A = \frac{1}{\sqrt{N}} \sqrt{\left(1 + \sum_{i=1}^{N-1} \cos\theta_i\right)^2 + \left(\sum_{i=1}^{N-1} \sin\theta_i\right)^2} \tag{34}$$

and the phase shift $\phi = \arcsin\left(\sqrt{N}\sum_{i=1}^{N-1}\sin\theta_i/A\right)$. Similarly, we obtain $F'(\theta_b) = -(2\pi/l)\sqrt{N}A\sin(\theta_b + \phi)$. So $\gamma(\theta_b, \{\theta_i\})$ can be written as a cosine function

$$\gamma(\theta_b; \{\theta_i\}) = NP_y^0 + \sqrt{N} A \, P_\gamma \cos(\theta_b + \phi + \varphi) \tag{35}$$

where

$$P_\gamma = a\sqrt{\left(P_y^0\right)^2 + \left(2\pi P_\sigma \Delta x_b/l\right)^2} \tag{36}$$

$$= aP_0^y \sqrt{1 + \left(\frac{2\pi\sigma}{\tau_y l}\right)^2} \tag{37}$$

and $\varphi = -\arccos\left(P_0^y / P_\gamma\right)$, from which it's easy to see that the pressure threshold is

$$\Delta P_c = NP_y^0 + \sqrt{N} A\, P_\gamma \tag{38}$$

$$= P_y^0 \left[N + a\sqrt{N} A \sqrt{1 + \left(\frac{2\pi\sigma}{\tau_y l}\right)^2} \right] \tag{39}$$

We now discuss three different possible cases related to different configurations of the blobs positions:

- Each blob is separated from its nearest neighbours by a distance equal to the spatial period l, namely $\theta_i = 0 \; \forall \; i$. This implies that $A = \sqrt{N}$, and ΔP_c reaches the highest possible value

$$\Delta P_c = N\left(P_y^0 + P_\gamma\right) \tag{40}$$

- Each blob is separated from its nearest neighbours by half of the spatial period $l/2$, so $\theta_i = \pi$ for i odd and $\theta_i = 2\pi$ for i even. It follows that $A = 0$ if N is even, or $A = 1$ if N is odd, and ΔP_c takes the lowest possible value

$$\Delta P_c = \begin{cases} NP_y^0 & \text{if } N \text{ even} \\ \\ NP_y^0 + P_\gamma & \text{if } N \text{ odd} \end{cases} \tag{41}$$

- The position of every blob is uniformly distributed along the tube. This is equivalent to suppose that all the $N-1$ angular differences θ_i are uniformly distributed in the interval $[0, 2\pi]$. In the limit of N sufficiently large, A follows, in the interval $[0, +\infty[$, the probability distribution

$$\Pi(A) = 2A\, e^{-A^2}. \tag{42}$$

In order to prove eq. (42), we first calculate the probability distribution of the variable $B = NA^2$:

$$g(B) = \frac{1}{(2\pi)^{N-1}} \int_0^{2\pi} d\theta_1 \cdots \int_0^{2\pi} d\theta_{N-1}\, \delta\left(B - NA^2\right). \tag{43}$$

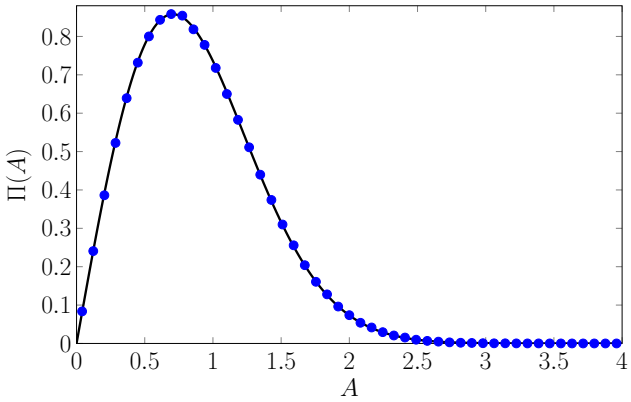

Fig. 6 Probability distribution of the amplitude A defined in equation (34). Blue dots represent the histogram of 10^6 numerical samplings of A, each obtained generating $N = 1000$ values of θ_i uniformly distributed in $(0, 2\pi)$; the samplings are collected in 50 bins of equal size in the domain $[0, 4]$. The solid line is the analytical prediction given by equation (46).

To solve (43) it's convenient to perform a Laplace transform:

$$\begin{aligned}\widetilde{g}(s) &= \int_0^{+\infty} dB\; e^{-sB} g(B) \\ &= \frac{1}{(2\pi)^{N-1}} \int_0^{2\pi} d\theta_1 \cdots \int_0^{2\pi} d\theta_{N-1}\, e^{-s\left(\left(1+\sum_{i=1}^{N-1}\cos\theta_i\right)^2+\left(\sum_{i=1}^{N-1}\sin\theta_i\right)^2\right)}\end{aligned} \tag{44}$$

We define $m_x = \sum_{i=1}^{N-1} \cos\theta_i$ and $m_y = \sum_{i=1}^{N-1} \sin\theta_i$. Note that the average and the variance of both $\cos\theta_i$ and $\sin\theta_i$ in the interval $[0, 2\pi]$, are respectively 0 and 1/2. Moreover, their crossed integral (the covariance) in the same interval is zero, meaning that m_x and m_y are statistical independent. According to the central limit theorem, when $N - 1 \simeq N$ is sufficiently large, the distribution of both m_x and m_y is Gaussian with mean zero and variance $N/2$. Eq. (44) can be rewritten as

$$\begin{aligned}\widetilde{g}(s) &= \int_{-\infty}^{+\infty} dm_x \frac{e^{-\frac{m_x^2}{N}}}{\sqrt{\pi N}} \int_{-\infty}^{+\infty} dm_y \frac{e^{-\frac{m_y^2}{N}}}{\sqrt{\pi N}} e^{-s\left((1+m_x)^2+m_y^2\right)} \\ &= \frac{e^{-s+\frac{s^2}{1/N+s}}}{1+Ns} \xrightarrow{N\gg 1} \frac{1}{1+Ns}.\end{aligned} \tag{45}$$

The inverse Laplace transform leads to $g(B) = \exp(-B/N)/N$, from which eq. (42) follows directly.

From $\Pi(A)$ we get the distribution of ΔP_c in the interval $[NP_y^0, +\infty[$:

$$\Pi(\Delta P_c) = \frac{2(\Delta P_c - NP_y^0)}{NP_\gamma^2}\, e^{-\frac{\left(\Delta P_c - NP_y^0\right)^2}{NP_\gamma^2}}. \tag{46}$$

The mean flow rate per tube is finally obtained from (31) and using $\Delta P \to (NP_y^0)^+$ in eq. (46)

$$\overline{\langle q \rangle_T} \propto (\Delta P - NP_y^0)^{\frac{1}{n}+\frac{5}{2}}. \tag{47}$$

2.2 Beyond the sinusoidal geometry: the triangular saw tooth shape

In the previous section we computed explicitly the distribution of critical threshold (see equation (46)) for a tube tube with a sinusoidal deformation and random located identical blobs. In particular it comes out that the distribution vanishes linearly at NP_y^0. How general is this result?
We can prove that the result is still robust if the N blobs have slightly different sizes (see Appendix A). However, in this section we show that the shape of the distribution is very sensitive to the analytical properties of $f(x)$. As an important example, we discuss in detail the triangular saw tooth shape introduced in eq. (23), and we first focus on the fully Newtonian case (for which $\tau_y = 0$), and then on the non-Newtonian blobs case but where capillarity effects can be neglected (for which $\sigma = 0$).

2.2.1 Blobs of Newtonian fluid

If the tube is non uniform, even Newtonian blobs lead to a critical pressure ΔP_c, due to the capillary pressure drop at the interface. The value of ΔP_c corresponds to the global maximum, in the interval $0 \le x_b < l$, of the function $\gamma(x_b/r_0)$, expressed by equation (27), with $P_y^0 = 0$, namely

$$\Delta P_c = \sqrt{N} A P_\gamma, \tag{48}$$

where

$$A = \frac{1}{\sqrt{N}} \frac{l}{4r_0} \max_{0 \le x_b < l} \left| F'\left(\frac{x_b}{r_0}; \left\{\frac{x_i}{r_0}\right\}\right)\right| \tag{49}$$

and $P_\gamma = (4r_0/l) a P_\sigma \Delta x_b$. We remind that $F'(y; \{\frac{x_i}{r_0}\})$ is the first derivative of Eq. (28) with respect to y, and can be seen as the sum of N contributions. For the triangular saw tooth shape, there is a contribution $-4r_0/l$ for every blob located in the semi-period interval $[0, l/2]$ and $+4r_0/l$ for every blob in the other semi-period $[l/2, l]$. When x_b moves from 0 to l, all the blobs are shifted of the same quantity. The function $\gamma(\frac{x_b}{r_0}; \{\frac{x_i}{r_0}\})$ remains constant until one of the two facts occurs: either the most right blob belonging to the first semi-period enters the second, so that the function γ increases by $2P_\gamma$, or the last blob belonging to the second semi-period enters the first, so that γ

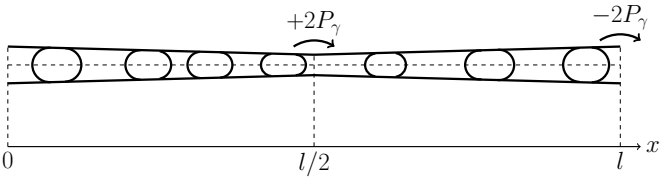

Fig. 7 Sketch of several blobs in a tube presenting the triangular modulation given by eq. (23).

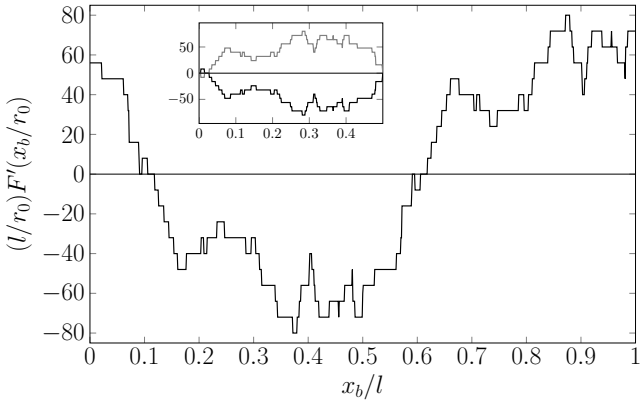

Fig. 8 Plot of a typical $F'(x_b/r_0)$, obtained from eq. (23) and (28), in a triangular tube with $N = 50$ blobs uniformly distributed in $(0, l)$. Here we set $l = 1$. The two bridges are shown separately in the inset.

decreases by $-2P_\gamma$. A sketch of this procedure is shown in figure 7. Increasing x_b further, other jumps occur for every blob entering in a new semi-period. γ corresponds then to a 1-dimensional *simple random walk* (Weiss, 1996), a process in which, for each of the N steps corresponding to the N blobs, γ will perform a stepwise increment of $\pm 2P_\gamma$. Since the probability for a blob to be in the first or second semi-period is the same, γ can increase by $2P_\gamma$ or $-2P_\gamma$ with equal probability, so this random walk is symmetric with a diffusion coefficient of $D = 2P_\gamma^2$. Moreover, due to the periodicity of the system, this random walk is periodical of period l. A typical trajectory is shown in figure 8. The random walk displays the symmetry $\gamma\left(\frac{x_b}{r_0}; \left\{\frac{x_i}{x_0}\right\}\right) = -\gamma\left(\frac{l/2+x_b}{r_0}; \left\{\frac{x_i}{x_0}\right\}\right)$ and can be decomposed into two Brownian bridges with mirror symmetry, namely two Brownian processes constraint to both start and end at 0 and with opposite sign. If we denote the two processes $z_1(i)$ and $z_2(i)$, they evolve from $i = 0$, in which $z_1(0) = z_2(0) = 0$, to $i = N$, in which $z_1(N) = z_2(N) = 0$; the two bridges are identical but opposite in sign, namely $z_1(i) = -z_2(i)$. As a consequence, equation (49) can be written as

$$A = \frac{1}{\sqrt{N}} \frac{l}{4r_0} \max_{0<i<N} |z_1(i)| \tag{50}$$

The exact calculation of the distribution of A can be done using the methods discussed in Mori et al (2020) for Brownian bridges. However, the statistical behaviour of $\max_{0<i\leq N}|z_1(i)|$ should be similar to the one of the span S of the process, defined as $S = \max_{0<i\leq N}(z_1) - \min_{0<i\leq N}(z_1)$. For the span, rigorous results are proven not only for the Brownian motion but for Gaussian processes with generic Hurst exponent H (the Brownian motion corresponds to $H = 1/2$). In particular, the probability to have a small span ε is known to vanish singularly as

$$\text{Prob}[S < \varepsilon] \propto e^{-\frac{kN}{\varepsilon^{1/H}}} \quad \text{for} \quad \varepsilon \to 0, \tag{51}$$

where k is a numerical prefactor of order one (Dean et al, 2014). From eq. (51), we can infer that the probability distribution of A vanishes as

$$\Pi(A) \propto A^{-3} e^{-\frac{k}{A^2}} \quad \text{for} \quad A \to 0. \tag{52}$$

The presence of an essential singularity at the origin indicates that the tubes with small critical pressure are extremely rare. From (52) it follows that the probability distribution of ΔP_c goes as

$$\Pi(\Delta P_c) \propto (\Delta P_c)^{-3} e^{-\frac{2kNP_\gamma^2}{(\Delta P_c)^2}} \quad \text{for} \quad \Delta P_c \to 0. \tag{53}$$

From eq. (31) we then find that, in the limit of small ΔP, the mean flow rate per tube vanishes exponentially as

$$\overline{\langle q \rangle_T} \propto e^{-\frac{2kNP_\gamma^2}{\Delta P^2}}. \tag{54}$$

2.2.2 Blobs of yield stress fluid without capillary effects

The same approach allows to solve the case of blobs of Non-Newtonian fluid for which we neglect capillary effects. The value of ΔP_c corresponds to the maximum, in the interval $0 < x_b < l$, of (27) with $P_\sigma = 0$, namely

$$\Delta P_c = NP_y^0 + \sqrt{N} A P_\gamma \tag{55}$$

where

$$A = \frac{1}{\sqrt{N}} \max_{0\leq x_b<l} \left| F\left(\frac{x_b}{r_0}; \left\{\frac{x_i}{r_0}\right\}\right)\right| \tag{56}$$

and $P_\gamma = aP_y^0$. Here $F\left(\frac{x_b}{r_0}, \left\{\frac{x_i}{r_0}\right\}\right)$ is the integral of the random walk discussed in the Newtonian case. A typical trajectory is shown in figure 10 and corresponds to the trajectory of a Random Acceleration Process (RAP) (Burkhardt, 2007), a piecewise linear function where the slope performs a Random walk; in particular, this Gaussian process represents the integral of a Brownian Bridge,

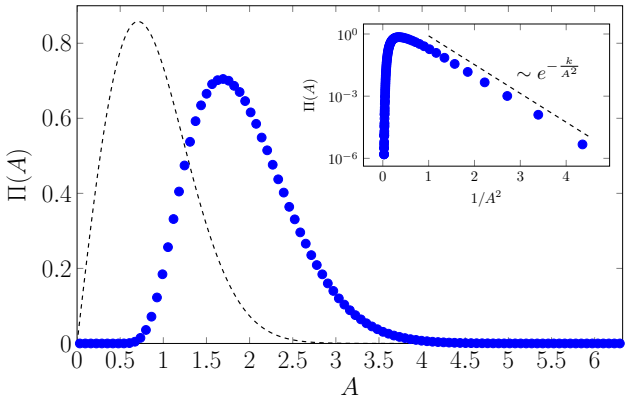

Fig. 9 Distribution of A for a train of blobs of Newtonian fluid in a triangular tube. Blue dots represent the histogram of 10^7 numerical samplings of A, each obtained generating $N = 1000$ values of blob positions and calculating (49); the samplings are collected in 100 bins of equal size in the domain $\left[0, 200/\sqrt{N}\right]$. The dashed curve is the probability distribution (46) valid for a sinusoidal tube. In the inset, the numerical data $(A^{-2}, \Pi(A))$ are compared to the asymptotic trend of eq. (53) setting $k \simeq 3.2$.

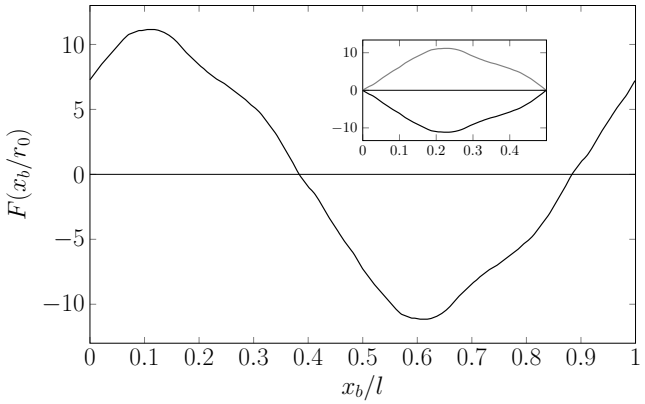

Fig. 10 Plot of a typical $F(x_b/r_0)$, obtained from eq. (23) and (28), in a triangular tube with $N = 50$ blobs uniformly distributed in $(0, l)$. Here we set $l = 1$. The two bridges are shown separately in the inset.

and is characterized by $H = 3/2$. The methods discussed in Majumdar et al (2010) may be a starting point for deriving an exact form for the distribution of the maximum of a RAP. However, following the lines of the previous discussion, we expect that the distribution of A vanishes at 0 as

$$\Pi(A) \propto \frac{1}{A^{5/3}} e^{-\frac{k^*}{A^{2/3}}} \quad \text{for} \quad A \to 0. \tag{57}$$

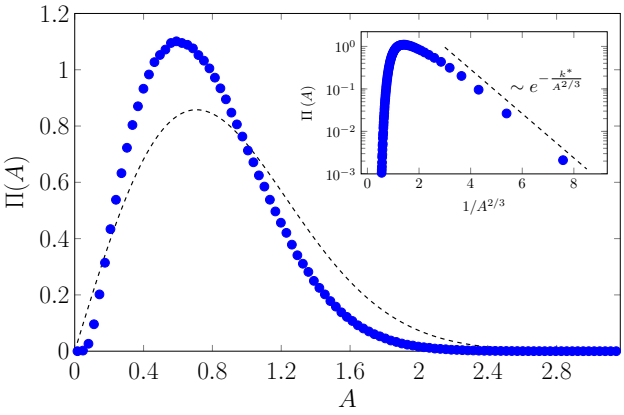

Fig. 11 Distribution of A for a train of blobs of yield stress fluid in a triangular tube neglecting capillary effects. Blue dots represent the histogram of 10^7 numerical samplings of A, each obtained generating $N = 1000$ values of blob positions and calculating (56); the samplings are collected in 100 bins of equal size in the domain $\left[0, 100/\sqrt{N}\right]$. The dashed curve is the probability distribution (46) valid for a sinusoidal tube. In the inset, the numerical data $(A^{-2}, \Pi(A))$ are compared to the asymptotic trend of eq. (53) setting $k^* \simeq 1.2$.

k^* is a numerical prefactor different from k. It follows that the distribution of the critical pressure vanishes at NP_y^0 as

$$\Pi(\Delta P_c) \propto (\Delta P_c - NP_y^0)^{-\frac{5}{3}} e^{-\frac{k^* N^{1/3} P_\gamma^{2/3}}{\left(\Delta P_y - NP_y^0\right)^{2/3}}} \quad \text{for} \quad \Delta P_c \to NP_y^0. \tag{58}$$

For $\Delta P \gtrsim NP_y^0$ the mean flow rate per tube scales now as

$$\overline{\langle q \rangle_T} \propto e^{-\frac{k^* N P_\gamma^{2/3}}{\left(\Delta P - NP_y^0\right)^{2/3}}}. \tag{59}$$

As a final remark we note that, as $H \to +\infty$ the function $\gamma\left(\frac{x_b}{r_0}, \left\{\frac{x_i}{r_0}\right\}\right)$ becomes smoother in x_b and the critical pressure distribution remains singular, but at a higher order of derivative. The linear behaviour in the limit $\Delta P_c \to 0$ found for the sinusoidal case represents then the most regular behaviour we can expect.

3 Conclusion

In this paper, we studied the flow rate curve in tubes filled with a Newtonian fluid and where blobs of non-Newtonian (or Newtonian) fluid are injected.

One blob. When a single blob is injected, we found a yield pressure threshold ΔP_c below which there is no flow. Above this threshold, the flow Q is strongly

non-linear and grows with a characteristic exponent:

$$Q(\Delta P) \propto (\Delta P - \Delta P_c)^{\beta}. \tag{60}$$

The value of the threshold for the uniform tube of radius r_0 is: $\Delta P_c = P_y^0 = 2\tau_y \Delta x_b / r_0$, where τ_y is the yield stress of the non-Newtonian blob of size Δx_b. For a non-uniform tube of radius $r(x) = r_0/(1 + af(x/r_0))$, the value of the threshold is modified:

$$\Delta P_c = P_y^0 + P_\gamma, \tag{61}$$

where the value of P_γ depends on the geometry of the tube. The exponent β depends on both the rheology and the geometry of the tube. Its value has been summarised in table 1.
Concerning P_γ, we show that in general:

$$P_\gamma = a \max_{0<x_b<l} \left[P_y^0 f\left(\frac{x_b}{r_0}\right) + P_\sigma \frac{\Delta x_b}{r_0} f'\left(\frac{x_b}{r_0}\right) \right], \tag{62}$$

where P_σ is the contribution of the surface tension, and l is the length of the tube. Two special cases have been studied.

- Sinusoidal deformation, $f(x/r_0) = \cos(2\pi x/l)$:

$$\begin{aligned} P_\gamma &= a\sqrt{\left(P_y^0\right)^2 + \left(2\pi P_\sigma \Delta x_b / l\right)^2} \\ &= a P_y^0 \sqrt{1 + \left(\frac{2\pi\sigma}{\tau_y l}\right)^2} \end{aligned} \tag{63}$$

  In this case, the function $\gamma(x/r_0)$ is regular around the maximum, so that $\beta = 1/2$ for the Newtonian case and $\beta = 1/2 + 1/n$ for the non-Newtonian one.
- Triangular deformation, $f(x/r_0) = \frac{4r_0}{l}\left|\frac{x}{r_0} - \frac{l}{2r_0}\right| - 1$:

$$\begin{aligned} P_\gamma &= a\left(2P_y^0 + \frac{4\Delta x_b}{l} P_\sigma\right) \\ &= 2aP_y^0\left(1 + \frac{2\sigma}{\tau_y l}\right) \end{aligned} \tag{64}$$

  In this case, the function $\gamma(x/r_0)$ is singular around the maximum ($\delta = 1$), so that $\beta = 0$ for the Newtonian case and $\beta = 1/n$ for the non-Newtonian one.

N blobs. In the case of the uniform tube, the flow curve is identical as for the single blob. The value of the threshold coincides with the one of a single blob with the same amount of fluid. The case of a non-uniform tube is instead more interesting. The value of the pressure threshold ΔP_c depends explicitly

	Newt	Non-Newt
Uniform	$\beta = 1$	$\beta = 1/n + 1$
Non-uniform	$\beta = 1/2$	$\beta = 1/n + 1/2$

Table 1 Summary of the exponent β when a single blob is injected in a tube filled with a Newtonian fluid. In the case of a non-uniform tube, $\gamma(x/r_0)$ is assumed regular around the maximum, i.e. $\gamma(x/r_0) \sim \Delta P_c + \alpha(x - x_m)^2$. Otherwise, if $\gamma(x/r_0) \sim \Delta P_c + \alpha(x - x_m)^\delta$, the exponent are $\beta = 1 - 1/\delta$ and $\beta = 1 + 1/n - 1/\delta$ for the Newtonian and non-Newtonian case respectively.

on the number of blobs and their relative distance. Assuming that the blobs are identical and evenly distributed, we show that ΔP_c can be written as

$$\Delta P_c = N P_y^0 + \sqrt{N} A P_\gamma, \tag{65}$$

where A is a non-dimensional positive random variable of order 1. The probability distribution of A depends on the tube shape.
We studied the following particular cases:

- Sinusoidal deformation, $f(x) = \cos \frac{2\pi}{x} l$. We found an explicit formula for $\Pi(A)$, valid in the limit of many blobs

$$\Pi(A) = 2Ae^{-A^2}. \tag{66}$$

- Triangular deformation, $f(x/r_0) = \frac{4r_0}{l}\left|\frac{x}{r_0} - \frac{l}{2r_0}\right| - 1$. We don't have an explicit formula for $\Pi(A)$, but we show how $\Pi(A)$ vanishes when $A \to 0$, in two limiting cases:

  1. Newtonian fluid:

$$\Pi(A \to 0) \propto \frac{1}{A^3} e^{-\frac{k}{A^2}}, \tag{67}$$

     where k is a numerical constant.
  2. Non-Newtonian fluid neglecting capillary effects:

$$\Pi(A \to 0) \propto \frac{1}{A^{5/3}} e^{-\frac{k^*}{A^{2/3}}}, \tag{68}$$

     where k^* is another numerical constant.

Concerning the flow, for a fiber bundle model and in the limit of many tubes, the total flow curve results from averaging all the blobs position configurations. It can be written in the form:

$$\overline{Q(\Delta P)} \propto \left(\Delta P - N P_y^0\right)^\beta, \tag{69}$$

where the overline stands for an average over all blobs configurations. The values obtained for the exponent β are given in table 2.

	Newt	Non-Newt
Uniform	$\beta = 1$	$\beta = 1/n + 1$
Sinusoidal	$\beta = 5/2$	$\beta = 1/n + 5/2$

Table 2 Summary of the exponent β when many blobs are injected in a tube filled with a Newtonian fluid. If the tube is uniform, we recover the result of a single blob. If the tube has a sinusoidal shape, the exponent is modified.

It is important to remark that within the fiber bundle model, the value of β depends explicitly on the regularity of the function $\gamma(x)$. For example, in the triangular case, $\beta = 0$ and the flow displays an essential singularity:

$$\overline{Q(\Delta P)} \propto e^{-\frac{k}{\left(\Delta P - N P_y^0\right)^{1/H}}}, \tag{70}$$

the Hurst exponent H characterizes the self-affine behavior of the function $\gamma(x)$. For example, we showed that in the triangular geometry $H = 1/2$ for a Newtonian fluid and $H = 3/2$ for a non-Newtonian fluid with negligible capillarity. One can wonder if this dependence holds also for a realistic porous media. Indeed, the fiber bundle model is a crude approximation as all tubes are independent. A challenge for future works is then to solve the flow in frameworks of interacting tubes.

References

Al-Fariss T, Pinder KL (1987) Flow through porous media of a shear-thinning liquid with yield stress. Can J Chem Eng 65(3):391–405. https://doi.org/10.1002/cjce.5450650306

Aursjø O, Erpelding M, Tallakstand KT, et al (2014) Film flow dominated simultaneous flow of two viscous incompressible fluids through a porous medium. Front Physics 2:63. https://doi.org/10.3389/fphy.2014.00063

Balhoff MT, Thompson KE (2004) Modeling the steady flow of yield-stress fluids in packed beds. AIChE J 50(12):3034–3048. https://doi.org/10.1002/aic.10234

Barbati AC, Desroches J, Robisson A, et al (2016) Complex fluids and hydraulic fracturing. Annual Review of Chemical and Biomolecular Engineering 7(1):415–453. https://doi.org/10.1146/annurev-chembioeng-080615-033630

Barnes H, Hutton J, Walters K (1989) An introduction to rheology, vol 3. Elsevier Science Limited, New York, NY

Bauer D, Talon L, Peysson Y, et al (2019) Experimental and numerical determination of Darcy's law for yield stress fluids in porous media. Phys Rev Fluids 4:063,301. https://doi.org/10.1103/PhysRevFluids.4.063301

Bear J (1988) Dynamics of Fluids in Porous Media. Elsevier, New York, NY

Bessonov N, Sequeira A, Simakov S, et al (2016) Methods of blood flow modelling. Mathematical modelling of natural phenomena 11(1):1–25. https://doi.org/10.1051/mmnp/201611101

Bird R, Armstrong R, Hassager O (1987) Dynamics of polymeric liquids. Vol. 1, 2nd Ed. : Fluid mechanics. John Wiley and Sons Inc., New York, NY

Bird RB (1976) Useful non-Newtonian models. Annual Review of Fluid Mechanics 8(1):13–34. https://doi.org/10.1146/annurev.fl.08.010176.000305

Brown SR (1987) Fluid flow through rock joints: The effect of surface roughness. Journal of Geophysical Research: Solid Earth 92(B2):1337–1347. https://doi.org/10.1029/JB092iB02p01337

Burkhardt TW (2007) The random acceleration process in bounded geometries. Journal of Statistical Mechanics: Theory and Experiment 2007(07):P07,004–P07,004. https://doi.org/10.1088/1742-5468/2007/07/p07004

Chen M, Rossen W, Yortsos YC (2005) The flow and displacement in porous media of fluids with yield stress. Chem Eng Sci 60(15):4183 – 4202. https://doi.org/10.1016/j.ces.2005.02.054

Chevalier T, Talon L (2015) Generalization of Darcy's law for Bingham fluids in porous media: From flow-field statistics to the flow-rate regimes. Phys Rev E 91:023,011. https://doi.org/10.1103/PhysRevE.91.023011

Chevalier T, Salin D, Talon L, et al (2015) History effects on nonwetting fluid residuals during desaturation flow through disordered porous media. Phys Rev E 91:043,015. https://doi.org/10.1103/PhysRevE.91.043015

Coussot P (2005) Rheometry of pastes, suspensions, and granular materials: applications in industry and environment. John Wiley and Sons, New York, NY

Dean DS, Gupta S, Oshanin G, et al (2014) Diffusion in periodic, correlated random forcing landscapes. Journal of Physics A: Mathematical and Theoretical 47(37):372,001. https://doi.org/10.1088/1751-8113/47/37/372001

Dullien FA (1991) Porous media: fluid transport and pore structure. Academic press, Cambridge, MA

Entov V (1967) On some two-dimensional problems of the theory of filtration with a limiting gradient. Prikl Mat Mekh 31:820–833. https://doi.org/10.

1016/0021-8928(67)90120-7

Fraggedakis D, Chaparian E, Tammisola O (2021) The first open channel for yield-stress fluids in porous media. Journal of Fluid Mechanics 911:A58. https://doi.org/10.1017/jfm.2020.1105

Frigaard I, Ryan D (2004) Flow of a visco-plastic fluid in a channel of slowly varying width. Journal of Non-Newtonian Fluid Mechanics 123(1):67–83. https://doi.org/https://doi.org/10.1016/j.jnnfm.2004.06.011

Happel J, Brenner H (1983) Low Reynolds number hydrodynamics. D. Reidel Publishing Co., Hingham, MA

Liu C, De Luca A, Rosso A, et al (2019) Darcy's law for yield stress fluids. Phys Rev Lett 122:245,502. https://doi.org/10.1103/PhysRevLett.122.245502

Lopez X, Valvatne PH, Blunt MJ (2003) Predictive network modeling of single-phase non-Newtonian flow in porous media. J Colloid Interface Sci 264(1):256 – 265. https://doi.org/https://doi.org/10.1016/S0021-9797(03)00310-2

Majumdar SN, Rosso A, Zoia A (2010) Time at which the maximum of a random acceleration process is reached. Journal of Physics A: Mathematical and Theoretical 43(11):115,001. https://doi.org/10.1088/1751-8113/43/11/115001

Malevich A, Mityushev V, Adler P (2006) Stokes flow through a channel with wavy walls. Acta mechanica 182(3-4):151–182

Mori F, Majumdar SN, Schehr G (2020) Distribution of the time between maximum and minimum of random walks. Physical Review E 101(5). https://doi.org/10.1103/physreve.101.052111

Nash S, Rees DS (2016) The effect of microstructure on models for the flow of a Bingham fluid in porous media. Transp Porous Media https://doi.org/10.1007/s11242-016-0813-9

Park H, Hawley M, Blanks R (1973) The flow of non-Newtonian solutions through packed beds. SPE 15(11):4722. https://doi.org/10.1002/pen.760151102

Popel AS, Johnson PC (2005) Microcirculation and hemorheology. Annual Review of Fluid Mechanics 37(1):43–69. https://doi.org/10.1146/annurev.fluid.37.042604.133933

Rassi EM, Codd SL, Seymour JD (2011) Nuclear magnetic resonance characterization of the stationary dynamics of partially saturated media during

steady-state infiltration flow. New Journal of Physics 13(1):015,007–. https://doi.org/10.1088/1367-2630/13/1/015007

Rodríguez de Castro A, Radilla G (2017) Non-Darcian flow of shear-thinning fluids through packed beads: Experiments and predictions using forchheimer's law and ergun's equation. Advances in Water Resources 100:35 – 47. https://doi.org/10.1016/j.advwatres.2016.12.009

Roustaei A, Chevalier T, Talon L, et al (2016) Non-Darcy effects in fracture flows of a yield stress fluid. Journal of Fluid Mechanics 805:222–261. https://doi.org/10.1017/jfm.2016.491

Roux S, Herrmann HJ (1987) Disorder-induced nonlinear conductivity. Europhys Lett 4(11):1227. https://doi.org/10.1209/0295-5075/4/11/003

Roy S, Hansen A, Sinha S (2019) Effective rheology of two-phase flow in a capillary fiber bundle model. Frontiers in Physics 7:92. https://doi.org/10.3389/fphy.2019.00092

Scheidegger A (1953) Theoretical models of porous matter. Producers Monthly 17:17–23

Scheidegger A (1974) The physics of flow through porous media. University of Toronto Press

Sinha S, Hansen A (2012) Effective rheology of immiscible two-phase flow in porous media. Europhys Lett 99(4):44,004–. https://doi.org/10.1209/0295-5075/99/44004

Sinha S, Hansen A, Bedeaux D, et al (2013) Effective rheology of bubbles moving in a capillary tube. Phys Rev E 87:025,001. https://doi.org/10.1103/PhysRevE.87.025001

Sinha S, Bender AT, Danczyk M, et al (2017) Effective rheology of two-phase flow in three-dimensional porous media: Experiment and simulation. Transport in Porous Media 119(1):77–94. https://doi.org/10.1007/s11242-017-0874-4

Sochi T, Blunt M (2008) Pore-scale network modeling of Ellis and Herschel-Bulkley fluids. J Pet Sci Eng 60(2):105 – 124. https://doi.org/10.1016/j.petrol.2007.05.009

Tallakstad KT, Løvoll G, Knudsen HA, et al (2009) Steady-state, simultaneous two-phase flow in porous media: An experimental study. Phys Rev E 80:036,308. https://doi.org/10.1103/PhysRevE.80.036308

Talon L, Bauer D (2013) On the determination of a generalized Darcy equation for yield-stress fluid in porous media using a lattice-Boltzmann trt scheme. Eur Phys J E 36(12):139. https://doi.org/10.1140/epje/i2013-13139-3

Talon L, Auradou H, Hansen A (2014) Effective rheology of Bingham fluids in a rough channel. Front Physics 2(24):24. https://doi.org/10.3389/fphy.2014.00024

Waisbord N, Stoop N, Walkama DM, et al (2019) Anomalous percolation flow transition of yield stress fluids in porous media. Phys Rev Fluids 4:063,303. https://doi.org/10.1103/PhysRevFluids.4.063303

Weiss GH (1996) Random walks and random environments, volume 1: Random walks. Journal of Statistical Physics 82(5):1675–1677. https://doi.org/10.1007/BF02183400

Widmer Soyka RP, López A, Cecilia Persson C, et al (2013) Numerical description and experimental validation of a rheology model for non-Newtonian fluid flow in cancellous bone. Journal of the Mechanical Behavior of Biomedical Materials 27:43–53. https://doi.org/10.1016/j.jmbbm.2013.06.007

Xiong Y, Long X, Huang G, et al (2019) Impact of pore structure and morphology on flow and transport characteristics in randomly repacked grains with different angularities. Soils and Foundations 59(6):1992–2006. https://doi.org/https://doi.org/10.1016/j.sandf.2019.10.002

Yiotis AG, Talon L, Salin D (2013) Blob population dynamics during immiscible two-phase flows in reconstructed porous media. Phys Rev E 87:033,001. https://doi.org/10.1103/PhysRevE.87.033001

Yiotis AG, Dollari A, Kainourgiakis ME, et al (2019) Nonlinear Darcy flow dynamics during ganglia stranding and mobilization in heterogeneous porous domains. Phys Rev Fluids 4:114,302. https://doi.org/10.1103/PhysRevFluids.4.114302

Zhang Y, Bijeljic B, Gao Y, et al (2021) Quantification of nonlinear multiphase flow in porous media. Geophysical Research Letters 48(5). https://doi.org/10.1029/2020GL090477

Declarations

Author Contributions FL developed the theory and performed the analytical and numerical calculations. AR and LT helped in performing the analytical calculations. AH suggested the problem. All the authors contributed in writing the manuscript to its final form.

Funding This work was partly supported by the Research Council of Norway through its Center of Excellence funding scheme, project number 262644. Further support, also from the Research Council of Norway, was provided through its INTPART program, project number 309139. This work was also supported by "Investissements d'Avenir du LabEx" PALM (ANR-10-LABX-0039-PALM).

Conflict of interest The authors declare no conflict of interest.

A Blobs of different sizes in a tube with sinusoidal geometry

We generalize the study of the flow in a tube considering N blobs of different lengths. We call Δx_0 the size of the blob positioned at x_b and Δx_i the size of the blob at $x_b + x_i$, and for all i we take $\Delta x_i \ll l$. We also consider a radius variation small enough so that we can take every Δx_i constant. In the limit of small flow rate $q \to 0$, the pressure drop at the edges of the i-th blob is

$$P^+_{x_b+x_i} - P^-_{x_b+x_i+\Delta x_i} = \Delta x_i \left(\frac{q(x_b)}{C_0 r_0^{4+\frac{1}{n}}} \right)^{\frac{n}{n+1}} + P^0_{y,i} \left(1 + af\left(\frac{x_b + x_i}{r_0} \right) \right). \tag{71}$$

where $P^0_{y,i} = 2\tau_y \Delta x_i / r_0$. To this, one must add the capillary pressure drop $aP_\sigma \Delta x_i f'((x_b + x_i)/r_0)$. Summing the contributions of all the N blobs and neglecting the pressure drop induced by the Newtonian fluid, we obtain the following flow rate equation:

$$q(x_b, \{x_i\}; \{\Delta x_i\}) = C_0 r_0^{4+\frac{1}{n}} \left[\frac{\Delta P - \gamma\left(x_b/r_0; \{x_i/r_0\}, \{\Delta x_i\}\right)}{\sum_{i=0}^{N-1} \Delta x_i} \right]^{\frac{1}{n}+1}, \tag{72}$$

where

$$\begin{aligned} \gamma\left(\frac{x_b}{r_0}; \left\{ \frac{x_i}{r_0} \right\}, \{\Delta x_i\} \right) &= \sum_{i=0}^{N-1} P^0_{y,i} + \\ &+ a\left(\frac{2\tau_y}{r_0} G\left(\frac{x_b}{r_0}; \left\{ \frac{x_i}{r_0} \right\}, \{\Delta x_i\} \right) + \frac{P_\sigma}{r_0} G'\left(\frac{x_b}{r_0}; \left\{ \frac{x_i}{r_0} \right\}, \{\Delta x_i\} \right) \right) \end{aligned} \tag{73}$$

and the function

$$G\left(\frac{x_b}{r_0}; \left\{ \frac{x_i}{r_0} \right\}, \{\Delta x_i\} \right) = \Delta x_0 \, f\left(\frac{x_b}{r_0} \right) + \sum_{i=1}^{N-1} \Delta x_i \, f\left(\frac{x_b + x_i}{r_0} \right). \tag{74}$$

We now focus on the case of a tube presenting the sinusoidal modulation given by eq. (32). Defining $\theta_b = 2\pi x_b / l$ and $\theta_i = 2\pi x_i / l$, equation (74) can be written as a single sine function

$$G(x_b/r_0; \{x_i/r_0\}, \{\Delta x_i\}) = \sqrt{N} A \sin(\theta_0 + \phi) \tag{75}$$

with the amplitude

$$A = \frac{1}{\sqrt{N}} \sqrt{ \left(\Delta x_0 + \sum_{i=1}^{N-1} \Delta x_i \cos\theta_i \right)^2 + \left(\sum_{i=1}^{N-1} \Delta x_i \sin\theta_i \right)^2 }$$

and the phase shift $\phi = \arcsin\left(A^{-1}\sum_{i=1}^{N-1}\Delta x_i \sin\theta_i\right)$. Similarly, we obtain $G'(x_b;\{x_i\},\{\Delta x_i\}) = -\sqrt{N}A(2\pi/l)\sin(\theta_b+\phi)$. So $\gamma(\theta_b;\{\theta_i\},\{\Delta x_i\})$ can be written as:

$$\gamma(\theta_b;\{\theta_i\},\{\Delta x_i\}) = \sum_{i=0}^{N-1} P^0_{y,i} + \sqrt{N}A\,P'_\gamma\cos(\theta_b+\phi+\varphi), \tag{76}$$

where $P'_\gamma = a\sqrt{(2\tau_y/r_0)^2+(2\pi P_\sigma/l)^2}$ and $\varphi = -\arccos\left(2\tau_y/(r_0P'_\gamma)\right)$.The maximum of eq. (76) gives the pressure threshold

$$\Delta P_y = \sum_{i=0}^{N-1} P^0_{y,i} + \sqrt{N}A\,P'_\gamma. \tag{77}$$

We now suppose that every blob size is distributed uniformly between two extreme values Δx_m and Δx_M, with $\Delta x_\mathrm{m} < \Delta x_\mathrm{M} \ll l$. Then, for N sufficiently large, $\sum_{i=0}^{N-1} P^0_{y,i} = N\left\langle P^0_y\right\rangle$ with $\left\langle P^0_y\right\rangle = \tau_y\left(\Delta x_\mathrm{M}+\Delta x_\mathrm{m}\right)/r_0$. Moreover we assume the angular position θ_i to be distributed uniformly in the interval $[0,2\pi]$. It follows that the probability distribution $\Pi(A)$, in the domain $[0,+\infty[$, has the following expression:

$$\Pi(A) = \frac{2A}{q}\,e^{-\frac{A^2}{q}}; \tag{78}$$

here we define $q = (\Delta x_\mathrm{M}^2 + \Delta x_\mathrm{m}^2 + \Delta x_\mathrm{m}\Delta x_\mathrm{M})/3$. In particular, $\Pi(A)$ vanishes linearly as $A\to 0$. To prove (78), we calculate the probability distribution of the variable $B = NA^2$

$$\begin{aligned} g(B) = {} & \frac{1}{(2\pi)^{N-1}}\frac{1}{(\Delta x_\mathrm{M}-\Delta x_\mathrm{m})^N}\int_0^{2\pi} d\theta_1\ldots\int_0^{2\pi} d\theta_{N-1} \\ & \times\int_{\Delta x_\mathrm{m}}^{\Delta x_\mathrm{M}} d\Delta x_0\cdots\int_{\Delta x_\mathrm{m}}^{\Delta x_\mathrm{M}} d\Delta x_{N-1}\,\delta\left(B-NA^2\right). \end{aligned} \tag{79}$$

The Laplace transform of eq. (43) is

$$\begin{aligned} \widetilde{g}(s) = {} & \frac{1}{(2\pi)^{N-1}}\frac{1}{(\Delta x_\mathrm{M}-\Delta x_\mathrm{m})^N}\int_0^{2\pi} d\theta_1\ldots\int_0^{2\pi} d\theta_{N-1} \\ & \times\int_{\Delta x_\mathrm{m}}^{\Delta x_\mathrm{M}} d\Delta x_0\cdots\int_{\Delta x_\mathrm{m}}^{\Delta x_\mathrm{M}} d\Delta x_{N-1} e^{-s\left(\left(\Delta x_0+\sum_i\Delta x_i\cos\theta_i\right)^2+\left(\sum_i\Delta x_i\sin\theta_i\right)^2\right)}. \end{aligned} \tag{80}$$

We now define the statistical variables $m_x = \sum_{i=1}^{N-1}\Delta x_i\cos\theta_i$ and $m_y = \sum_{i=1}^{N-1}\Delta x_i\sin\theta_i$. The mean and variance of both $\Delta x_i\cos\theta_i$ and $\Delta x_i\sin\theta_i$ in the interval $[0,2\pi]\times[\Delta x_\mathrm{m},\Delta x_\mathrm{M}]$ are respectively 0 and $q/2$. m_x and m_y are

statistical independent since their covariance is zero. When $N-1 \simeq N$ is sufficiently large, the distribution of both m_x and m_y is Gaussian with mean zero and variance $Nq/2$. Eq. (80) becomes:

$$\begin{aligned}\widetilde{g}(s) &= \int_{-\infty}^{+\infty} dm_x \frac{e^{-\frac{m_x^2}{Nq}}}{\sqrt{\pi Nq}} \int_{-\infty}^{+\infty} dm_y \frac{e^{-\frac{3m_y^2}{Nq}}}{\sqrt{\pi Nq}} \int_{\Delta x_{\mathrm{m}}}^{\Delta x_{\mathrm{M}}} d\Delta x_0 \frac{e^{-s\left((\Delta x_0+m_x)^2+m_y^2\right)}}{\Delta x_{\mathrm{M}}-\Delta x_{\mathrm{m}}} \\ &= \frac{1}{(1+Nqs)} \int_{\Delta x_{\mathrm{M}}}^{\Delta x_{\mathrm{M}}} d\Delta_0 \frac{e^{-\Delta x_0^2\left(s-\frac{s^2}{\frac{1}{Nq}+s}\right)}}{\Delta x_{\mathrm{M}}-\Delta x_{\mathrm{m}}} \xrightarrow{N\gg 1} \frac{1}{1+Nqs}\end{aligned} \tag{81}$$

The Laplace inversion gives $g(B) = \exp(-B/(Nq))/(Nq)$, from which eq. (82) follows. From $\Pi(A)$ we get the distribution of ΔP_c in the interval $\left[N\left\langle P_y^0\right\rangle, +\infty\right]$:

$$\pi(\Delta P_y) = \frac{6(\Delta P_y - N\left\langle P_y^0\right\rangle)}{NqP'^2_\gamma} e^{-\frac{3\left(\Delta P_y - N\left\langle P_y^0\right\rangle\right)^2}{NqP'^2_\gamma}}. \tag{82}$$